JOURNAL OF MATERIALS SCIENCE 32 (1997) 4011–4017

Experimental evidence of crack tip shielding mechanisms in quasi-brittle materials

C. P. OSTERTAG
Department of Civil and Environmental Engineering, University of California, Berkeley, CA, 94720 USA

To gain insight into the shielding processes in quasi-brittle materials, *in situ* crack propagation and crack profile measurements were performed inside the scanning electron microscope (SEM). Crack tip shielding phenomena were studied in monolithic alumina and in SiC fibre-reinforced alumina matrix composites as a function of fibre coatings. The crack in the fibre-reinforced composite samples is bridged by a row of fibres which contains a fibre area fraction of 10%. The applied stress intensity factor necessary to extend the crack in the composite materials increased 25% for the gold coated fibre-reinforced alumina matrix composites and 13% for the polymer-coated fibre-reinforced composites, compared to the monolithic samples. Crack extension in the monolithic samples and in the fibre-reinforced composites occurred after the crack opening displacements close to the crack tip approached the critical crack tip profile corresponding to the intrinsic toughness of alumina. A hypothesis on the effect of closure stresses on crack profile shape and net toughness has been developed. Furthermore, crack profiles revealed that grain bridging in the vicinity of the fibres was operative in the fibre-reinforced composites at stress intensity factors far exceeding the critical stress intensity factor of the monolithic matrix material. The additional grain bridging in the vicinity of the fibres has never been reported and can only be revealed through crack profile measurements.

1. Introduction

The toughness increase in both monolithic alumina and fibre-reinforced composites is attributed to shielding processes in the crack wake [1–9]. The principal source of crack tip shielding in polycrystalline alumina is intergrain bridging across the crack interface behind the advancing crack front [1–4]. The micromechanics of grain bridging are that of a frictional pullout process in which the interlocking grains exert dissipative closure forces on the crack walls. Locked-in thermal expansion mismatch stresses in the alumina structure play a profound role in enhancing these pullout stresses, by clamping grains into the matrix. In fibre-reinforced composites the crack tip shielding results from fibres bridging the crack surfaces and the dissipative closure forces are due to elastic and frictional fibre bridging and frictional fibre pullout [6–9].

In situ crack propagation and crack profile measurements were performed inside the scanning electron microscope (SEM) to gain insight into the shielding processes. The shape of the crack profiles are strongly influenced by fibres bridging the crack and thereby exerting closure stresses on the crack walls. These closure stresses shield the crack tip from the applied load. In order for an existing crack to extend, a higher stress needs to be applied. The stress intensity factors associated with crack initiation and failure were investigated for both monolithic alumina samples and SiC fibre reinforced alumina matrix composites as a function of fibre coating.

The effect of closure stresses on reducing the crack tip stresses will be assessed through the crack opening displacement near the crack tip. The closure stresses that are operative in the composite samples lead to an additional toughening mechanism due to residual grain bridging in the vicinity of the fibres as will be discussed.

2. Experimental procedure

SiC fibre-reinforced composites and monolithic alumina samples were processed by tape casting. Coated SCS-6 SiC fibres (Textron Specialty Materials, MA) were placed between green tapes of monolithic material and cold pressed at 13 MPa. After a binder burnout procedure at 500 °C for 10 h, the specimens were pressureless sintered at 1600 °C for 2 h. The fibres were either polymer coated or gold coated before incorporating them into the matrix material. The polymer coating was used to avoid sintering stresses. It burns out at 500 °C, leaving a gap between the fibres and the matrix, which allows the matrix to shrink unconstrained by the surrounding fibres at the sintering temperature. The polymer burn-out process leaves the fibres coated with a thin carbon layer of 1 μm (in

0022–2461

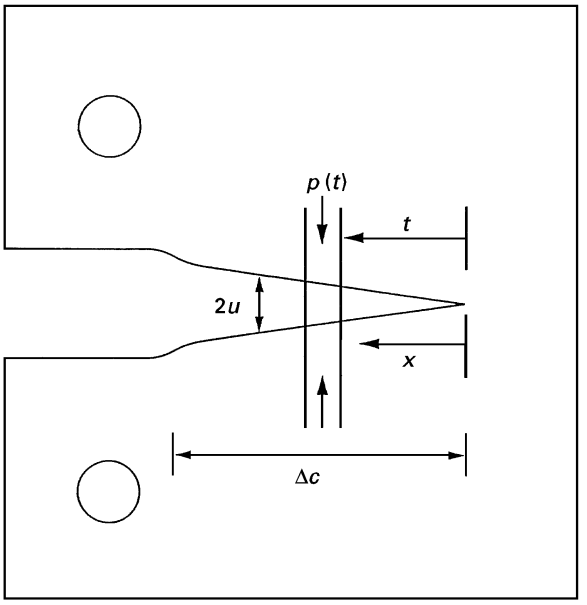

Figure 1 Schematic of compact tension specimen with row of fibres at position t behind the crack tip. Crack opening displacements $2u$ measured along the crack as a function of x behind the crack tip. Bridging traction $p(t)$ act to restrain the crack opening.

addition to the carbon rich surface layer of the SiC-6 SiC fibres). Fibres were also gold coated (60 nm in thickness) which prevents the fibre degradation often observed in polymer-coated fibre-reinforced composites with high fibre volume fractions and results in a higher frictional stress at the fibre–matrix interface compared to the polymer coating [10]. For detailed information on the processing of the tape casted composites and the coating procedure the reader is referred to reference [10].

Both the monolithic and the composite samples reached a final density of 92% after sintering at 1600 °C for 2 h. The samples contained elongated grains with a wide grain size distribution. The mean grain size was 12 μm.

Compact tension specimens were prepared for the *in situ* SEM crack propagation and crack profile measurements. The specimens conformed to ASTM standard geometry, with a width W of 15 mm and a thickness of 1.5 mm. The sample preparation, the precracking procedure, and the loading device used for the *in situ* SEM measurements are described in references [11, 12]. The samples were precracked in air and the crack extension of the through-thickness crack was observed inside the SEM. The samples have notch lengths between 3.5 and 3.9 mm. The composite samples were precracked to approximately 1800 μm. The crack in the composite samples is then bridged by a row of fibres in its wake at a distance t behind the crack tip, as schematically illustrated in Fig. 1. The row of fibres incorporates a fibre area fraction of 10%. In order to isolate the shielding contributions due to grain bridging from the shielding contribution due to fibre bridging, *in situ* crack propagation behaviour and crack profile measurements were conducted on monolithic alumina samples with approximately the same precrack lengths as those in the composite samples.

The crack opening displacements were recorded on video from the crack tip to the notch tip at a magnification of 30 000 × and then measured from the TV screen. Crack profiles were measured at different applied stress intensity factors, both before and after successive crack extensions. The cracks were rendered highly visible in the secondary electron mode by edge charging.

3. Results and discussion

3.1. Crack tip shielding

Bridging ligaments such as interlocking grains and fibres restrain the opening of the crack, as will be illustrated in the following sections and, consequently, cause a reduction in the stresses in the matrix near the crack tip. The reduction in stress at the crack tip is expressed as [7, 13]

$$K_{tip} = K_a - K_s \quad (1)$$

where K_{tip} is the local stress intensity factor at the crack tip, K_a is the applied stress intensity factor, and K_s the shielding stress intensity factor. The criterion for crack growth under monotonic loading is taken as the critical value of K_{tip} (i.e. $K_{tip} = T_o$, where T_o is the fracture toughness of the matrix material in the absence of shielding mechanisms). The corresponding critical value of K_a is the fracture toughness measured in the presence of shielding ($K_a = K_c = T_o + K_s$). Grain bridging in the monolithic samples and grains and fibres bridging the crack surfaces in the crack wake in the fibre-reinforced composites contribute to the shielding mechanisms in this study.

Crack tip shielding requires higher loads to be applied in order for the crack to initiate (i.e. extend from its precrack) and propagate a certain amount. The increase in toughness with crack length causes an increase in the crack growth resistance (R-curve) behaviour, which strongly affects the strength of components made from such quasi-brittle materials. The material strength is a function of the resistance curve (R-curve) and the initial crack length. Both the toughness and the strength can be influenced through microstructural design, however, they involve different choices of microstructures and interfacial frictional stresses at the fibre matrix interfaces, as will be discussed in Sections 3.5 and 3.6.

3.2. Crack tip shielding in monolithic samples

The crack initiated from the precrack on average at an applied stress intensity factor K_i of 4.7 MPa m$^{1/2}$ and the samples failed after stable crack extensions of 100 μm inside the SEM at the stress intensity factor $K_c = 5.1$ MPa m$^{1/2}$. K_i and K_c were obtained from the externally measured load using the stress intensity factor solution for compact tension specimens [14]. Crack profiles were measured to give some qualitative insight into the crack tip shielding mechanisms which affect the crack initiation resistance K_i (associated with crack initiation from the precrack) and the crack growth resistance with increasing crack length.

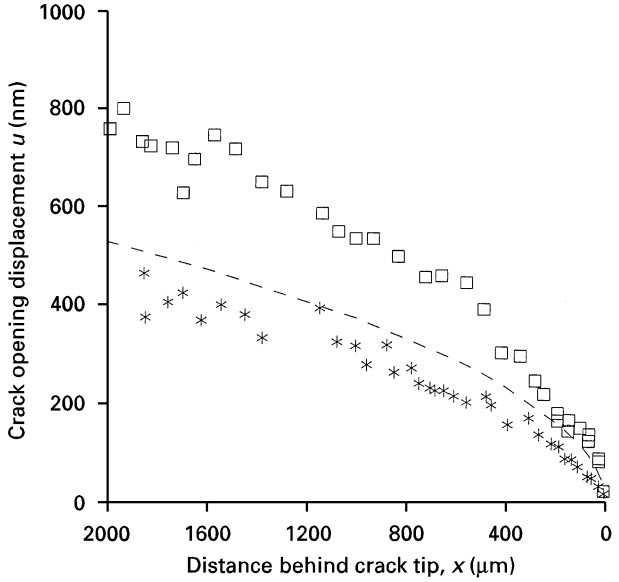

Figure 2 Crack profiles of monolithic alumina. Profile A (□) measured at $K_i = 4.7\ \text{MPa m}^{1/2}$ after crack extension, profile B (∗) measured at $K_a = 3.1\ \text{MPa m}^{1/2}$ before crack propagation occurred. Dashed line corresponds to $T_o = 2.7\ \text{MPa m}^{1/2}$.

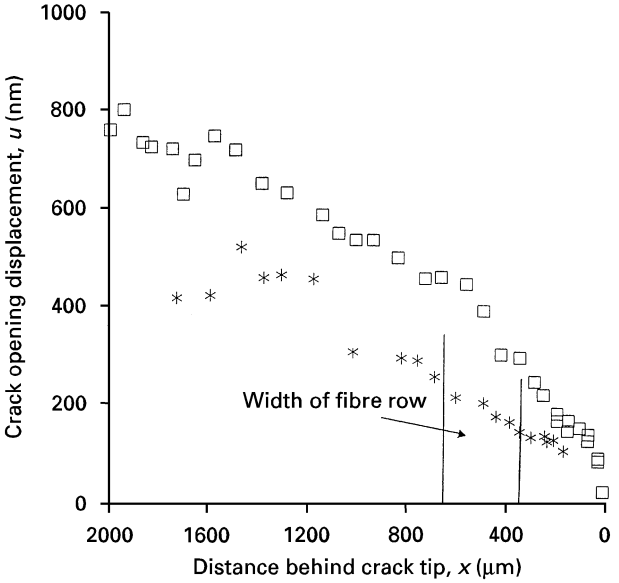

Figure 3 Crack profiles of monolithic (profile A, □) and gold-coated fibre-reinforced composite (profile B, ∗) at same applied stress intensity factor $K_a = 4.7\ \text{MPa m}^{1/2}$.

The crack profiles of a monolithic sample are shown in Fig. 2. Profile A was measured after the crack initiated from the precrack length at $K_a = K_i = 4.7\ \text{MPa m}^{1/2}$ and Profile B was measured at $K_a = 3.1\ \text{MPa m}^{1/2}$, where no crack extension has yet occurred.

The crack in the monolithic specimens propagated after the crack opening displacements in the vicinity of the crack tip (CTOD) reached a critical crack tip opening displacement $(\text{CTOD})_c$. The critical crack tip opening displacement fits the calculated crack tip profile for a stress intensity factor of $2.7\ \text{MPa m}^{1/2}$, which correlates closely to the intrinsic toughness of alumina [15]. The crack tip profile was calculated using the Irwin K-field plane strain displacement relation [16] and is indicated in Fig. 2 by the dashed line. The COD in the vicinity of the crack tip in profile B are below the CTOD corresponding to $2.7\ \text{MPa m}^{1/2}$ and therefore, the crack did not propagate yet. The shielding of the crack tip from the applied load resulted in an increase from $2.7\ \text{MPa m}^{1/2}$, (the intrinsic toughness of alumina) to $4.7\ \text{MPa m}^{1/2}$ at *constant* crack length. This crack initiation resistance due to crack tip shielding at constant crack length is even more pronounced in the fibre-reinforced composite materials.

3.3. Crack tip shielding in fibre-reinforced composites

Fig. 3 shows two crack profiles at the same applied stress intensity factor ($K_a = 4.7\ \text{MPa m}^{1/2}$). Profile A again corresponds to the monolithic sample discussed in Fig. 2. Profile B is for a gold-coated fibre-reinforced alumina matrix composite *before* any crack propagation occurred.

We first observe, from the crack profiles, the expected reduction in the crack opening displacement between the monolithic and composite material due to the presence of the fibres. Separation of the surfaces of a matrix crack which is bridged by uniaxially aligned fibres requires sliding of the matrix over the fibres. The sliding however is restricted by frictional forces. This restraining effect of the fibres causes a reduction in the crack surface displacement as observed, which is equivalent to applying a closure stress $p(t)$ onto the crack surfaces [7].

The fibres not only cause a reduction in the COD, but also a reduction in the crack tip stresses for a given applied load [7, 17]. Indeed, in the composite material a higher load was required for crack propagation to take place because the fibres shield the crack tip from the applied load. This in turn results in a reduced COD in the vicinity of the crack tip. In Fig. 4, the crack profile of the composite material at $K_a = 5.3\ \text{MPa m}^{1/2}$ (Profile C) is added to the two profiles at $K_a = 4.7\ \text{MPa m}^{1/2}$ of Fig. 3. Even at $5.3\ \text{MPa m}^{1/2}$ no crack extension took place in the composite material. The COD increased towards the notch tip (behind the row of fibres) but hardly changed between the fibre row and the crack tip. The fibres are clearly strong barriers to crack extension. Crack extension from the precrack was observed at $K_i = 5.9\ \text{MPa m}^{1/2}$, after the crack tip profile of the composite $(\text{CTOD})_{comp}$ approached the crack tip profile that resulted in crack initiation of the monolithic material. The closure stresses associated with the presence of a single row of fibres have therefore increased the applied stress intensity factor associated with crack initiation from $K_i = 4.7\ \text{MPa m}^{1/2}$ for the monolithic matrix material to $K_i = 5.9\ \text{MPa m}^{1/2}$ for the composite material at *constant* crack length.

Fibre coating can strongly influence the closure stresses and therefore the applied stress intensity factor necessary for crack propagation. Fig. 5 shows the profiles of Fig. 3 (monolithic sample profile (A) and gold-coated fibre composite sample profile (B)), to

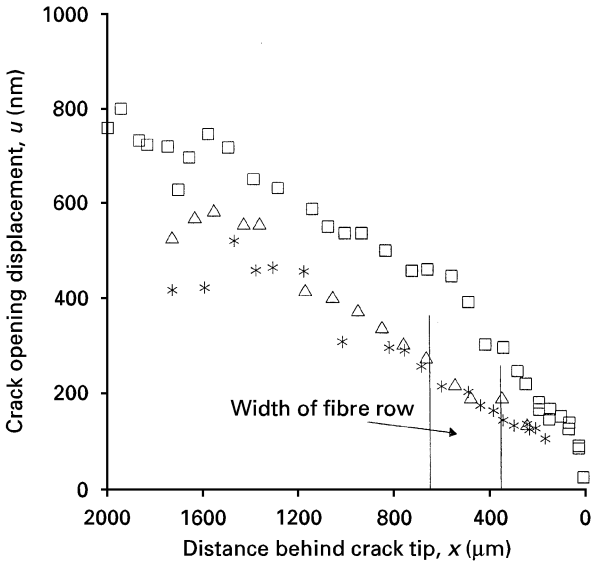

Figure 4 Crack profiles of monolithic alumina (profile A at $K_i = 4.7\ \mathrm{MPa\,m^{1/2}}$, □), and gold-coated fibre-reinforced composites (profile B at $K_a = 4.7\ \mathrm{MPa\,m^{1/2}}$, ∗ and profile C at $K_a = 5.3\ \mathrm{MPa\,m^{1/2}}$, △). Profiles B and C were measured before crack extension occurred.

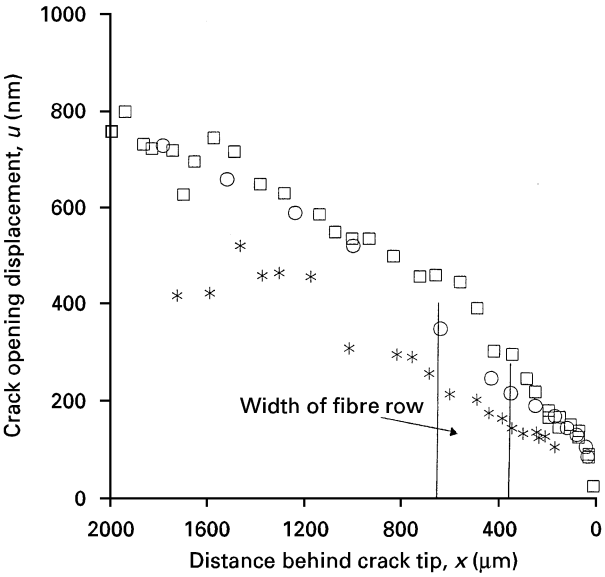

Figure 5 Crack profiles of monolithic alumina (profile A at $K_i = 4.7\ \mathrm{MPa\,m^{1/2}}$, □), gold-coated fibre-reinforced composite (profile B at $4.7\ \mathrm{MPa\,m^{1/2}}$, ∗), and polymer-coated fibre-reinforced composite (profile C at $4.9\ \mathrm{MPa\,m^{1/2}}$, ○). Profile C was measured after crack propagation.

which we have added the profile (C) of a polymer-coated fibre-reinforced composite sample with a single row of fibres at the same position t behind the crack tip as in profile B. The profile C was measured right after the crack propagated at $K_i = 4.9\ \mathrm{MPa\,m^{1/2}}$. The pull-out length in sample C exceeded that of sample B which suggests a lower interfacial frictional stress between the fibres and the matrix. The reduced interfacial friction is due to the carbon residue that remains at the fibres after the polymer burnout procedure. The polymer coated fibres were not as effective in shielding the crack tip from the applied load and the crack tip profile approached that of the monolithic material at a lower applied stress intensity factor compared to the samples with gold-coated fibres. The increase in K_i over the monolithic sample is only 13% for the polymer-coated fibre-reinforced composite, but 25% for the gold-coated fibre-reinforced composites. Furthermore, the polymer-coated fibre composite failed at $K_c = 5.3\ \mathrm{MPa\,m^{1/2}}$ while the gold-coated fibre composite failed at $K_c = 7.3\ \mathrm{MPa\,m^{1/2}}$. Based on our experimental results we have developed a hypothesis on the effect of closure stresses on both crack profile shape and net toughness which will be presented below.

3.4. A hypothesis on the influence of closure stresses on crack profile shape and net toughness

In this section we would like to propose a hypothesis for the behaviour of crack profiles in the presence of a single row of fibres for varying levels of closure stresses. The hypothesis is based on a generalization of the author's experimental measurements of crack profiles for samples with varying parameters.

Fig. 6a and b illustrate schematically crack profiles predicted by the hypothesis for several fibre-reinforced composite samples with one row of fibres at position t behind the crack tip. The dips in the curves represent the fibre positions. The profile indicated in Fig. 6a and b as "monolithic" corresponds to the monolithic matrix material at the onset of crack extension with the critical crack tip opening displacement. The composite profiles correspond to two hypothetical composite samples (labelled composite A and composite B), where composite B has a larger magnitude of closure stresses exerted at the crack walls by the row of fibres. The magnitude of closure stresses can be increased, for example, by increasing the interfacial friction τ between the fibres and the matrix.

Fig. 6a shows the predicted crack profiles for the same applied stress intensity factor. The three crack profiles correspond to the same length a and their COD coincide at the position between the loading holes (i.e. due to the same K_a). As might be intuitively expected, the COD is smallest at the fibre position for the sample with the highest closure stresses exerted on the crack walls due to fibre bridging (composite B). The magnitude of the closure stresses can be deduced from the difference in crack opening displacement Δu between the monolithic crack profile and the composite crack profile at position t behind the crack tip. The larger Δu, the larger the closure stresses. Accordingly, increasing closure stresses lead to a decrease in COD at the fibre position t as illustrated.

With increasing closure stresses the shielding of the crack tip by the applied load increases. Hence, the COD of the composite profiles in the vicinity of the crack tip is being reduced to below the critical crack tip opening displacement $(\mathrm{CTOD})_c$, which corresponds to T_o of the monolithic sample, which we will denote as $(\mathrm{CTOD})_{c\ \mathrm{matrix}}$. When the crack tip profile of the composite $(\mathrm{CTOD})_{\mathrm{comp}}$ coincides with the critical crack tip profile of the monolithic sample, crack

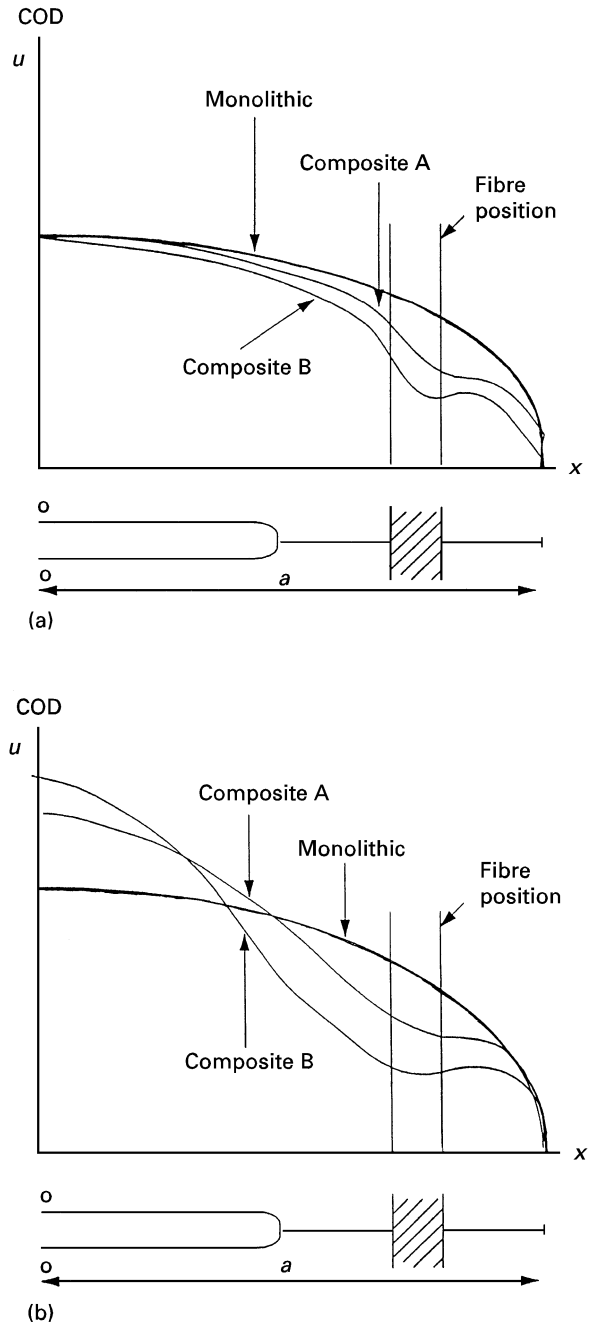

Figure 6 Schematic of crack profiles at crack length, a, for a monolithic material, and two composite materials (denoted at composite A and composite B). The closure stresses in composite B exceed the closure stresses of composite A at the fibre position. The dip in the composite profiles represents the fibre position. (a) Crack profiles of composite A and B before crack extension. All three crack profiles correspond to the same applied stress intensity factor K_a; (b) crack profiles of composites after crack extension at different K_a. Note larger COD at loading holes for composite B (due to larger closure stresses).

extension will occur. The larger the closure stresses, the more load has to be applied, in order for the crack tip profile of the composite to approach the $(CTOD)_{c\ matrix}$. This increase in applied load ultimately leads to an increase in toughness (and strength).

Fig. 6b shows the predicted crack profiles at the critical load for which crack extension occurred in each of the two composites. Here we submit that the profiles will cross each other at a point between the fibre position and the loading holes. Our experimental evidence indicates that the sample with largest closure stresses will have a smaller COD at the fibre position even though the applied load is largest. It is the author's belief that the common perception is that the larger the toughness, the larger the COD. Whereas this fact may be true at the loading holes, it certainly does not seem to be true at the fibre positions.

One of the important consequences of our hypothesis on the behaviour of crack profiles in the presence of closure stresses is that for composite materials whose matrix does exhibits R-curve behaviour (i.e Al_2O_3, Si_3N_4, SiC), closure stresses due to grain bridging are operative at applied stress intensity factors far exceeding the critical stress intensity factor K_c of the monolithic material. This additional toughening mechanism occurs because the COD has been constrained by the fibres to small enough values for the grains to still bridge the crack, even at applied loads which exceed the load necessary for failure of the monolithic material. The smaller the COD (i.e. the larger the closure stresses) the more important this additional factor becomes.

In summary, our hypothesis is that the larger the closure stresses, the more effective the crack tip shielding and the higher the crack initiation resistance K_i. Additionally, the larger the closure stresses, the smaller the COD at the fibre position allowing residual grain bridging to be effective.

3.5. Closure stresses influenced by interfacial frictional stress τ

Since the closure stresses seem to be the key factor in resisting crack initiation and thereby enhancing the toughness at constant crack length, we need to address what influences these closure stresses.

Closure stresses are strongly influenced by the interfacial frictional stress τ between the fibre and the matrix. The larger closure stresses leading to the small COD at the fibre position in composite B (Fig. 6) can be associated with a high interfacial frictional stress at the fibre/matrix interface.

Crack extension occurs after the COD in the crack tip region of the composite coincide with the critical CTOD of the matrix material. If we assume that (a) the fibres in the composites A and B fail at the same tensile stress and (b) that crack extension will occur before fibre failure, a higher applied stress is required to propagate the crack in composite B compared to composite A. This will lead to K_i of composite B exceeding K_i of composite A. This was experimentally observed for polymer and gold-coated fibre-reinforced composites, where the propagation of the former initiated at much lower K_i (Fig. 5). To increase K_i at constant crack length in the polymer-coated fibre-reinforced composites, more fibres have to be added to bridge the crack.

It should be appreciated that the increase in the interfacial frictional stress, while increasing the crack initiation resistance, may not lead to quasi-brittle behaviour, unless the load required for crack extension is smaller than the ultimate strength associated with the fibre bundle strength [18, 19]. For example, in

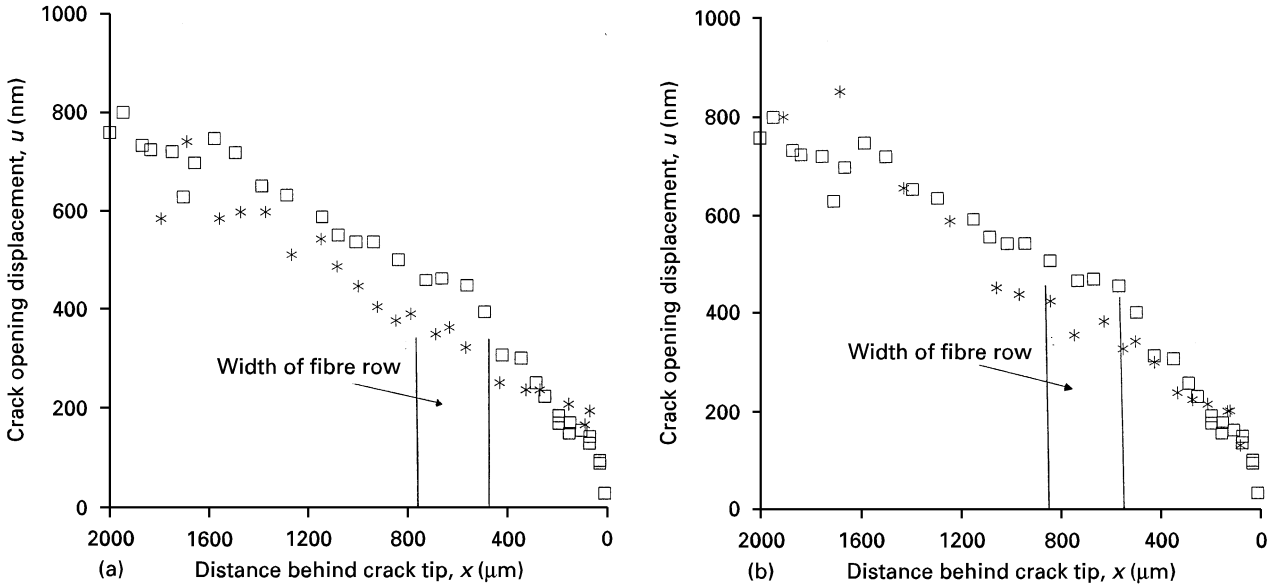

Figure 7 Crack profiles of monolithic and gold-coated fibre-reinforced composites after crack extension. (a) (□) Monolithic crack profile ($K_a = 4.7$ MPa m$^{1/2}$), (∗) composite crack profile measured at $K_a = 6.1$ MPa m$^{1/2}$; (b) (□) monolithic crack profile ($K_a = 4.7$ MPa m$^{1/2}$), (∗) composite crack profile measured at $K_a = 6.8$ MPa m$^{1/2}$.

uncoated fibre-reinforced composites, where the fibres were chemically bonded to the matrix, fibre failure occurred at the onset of crack extension, leading to catastrophic, brittle failure [11]. With increasing τ, the axial stress in the fibre decays rapidly with distance from the matrix crack plane, resulting in fibre failure at locations close to the crack plane and hence closely behind the crack tip. For composites with a low interfacial frictional stress the bridging stress supported by the fibres increases more slowly with distance behind the crack tip, and a longer bridging zone is developed behind the crack tip. An optimum τ is required which leads to crack initiation resistance K_i and allows for a fibre bridging zone to develop behind the crack tip.

3.6. Toughness increase with increasing crack length

After the initial crack resistance the crack propagates in a stable manner and the associated crack profiles after each propagation are shown in Fig. 7a and b at $K_a = 6.1$ MPa m$^{1/2}$ and $K_a = 6.8$ MPa m$^{1/2}$, respectively, together with the monolithic crack profile at $K_i = 4.7$ MPa m$^{1/2}$. Note that after crack propagation, the crack tip profiles of the composite samples coincide with the crack tip profile of the monolithic material. The composite failed at $K_c = 7.3$ MPa m$^{1/2}$.

The influence of fibres on crack tip shielding decreases with increasing distance of the fibre row from the crack tip. However, if during crack propagation, the crack encounters a second row of fibres, the crack growth resistance will be enhanced further due to the interaction of the second row of fibres with the crack tip region. Some preliminary results on the crack interaction with a second row of fibres reveal that the crack opening displacements in the vicinity of the crack tip again are smaller than the $(CTOD)_c$ of the monolithic alumina. If the fibre rows are spaced too far apart, the COD reduction in the vicinity of the crack tip is mainly due to the second row of fibres. However, if the fibre row spacing is small enough, the closure stresses due to the two rows of fibres are cumulative. Therefore, the crack growth resistance will increase with increasing crack length if the crack is bridged by closely spaced multiple rows of fibres.

4. Summary

1. The toughness increase in SiC fibre-reinforced alumina matrix composites is attributed to bridging mechanisms which shield the crack tip from the applied load. The fibres and the grains restrain the opening of the crack by exerting closure stresses on the crack walls, which cause a reduction in the crack tip stresses. The reduction in crack tip stresses due to fibres and grains bridging the crack wake was assessed through crack profile measurements. In the fibre-reinforced composites, crack extension occurs after the COD in the vicinity of the crack tip coincides with the critical CTOD corresponding to the intrinsic toughness of the alumina matrix material.

2. The toughness increase in both the monolithic samples and the fibre-reinforced composites is attributed to two contributions: the crack initiation resistance (i.e. at constant crack length) and the crack propagation resistance (i.e. with increasing crack length). The applied stress intensity factor necessary for crack extension was investigated for both monolithic samples and fibre-reinforced composites with 10% fibre area fractions. The study reveals that the crack initiation resistance, K_i, strongly depends on the closure stresses exerted on the crack walls due to fibre and grain bridging. In the fibre-reinforced composites these closure stresses were influenced through fibre coating. The higher K_i for gold-coated fibre-reinforced

composites compared to the polymer-coated composites suggests higher frictional stresses between the fibre/matrix interface. For the polymer-coated fibre-reinforced composites to reach the same net toughness as the gold-coated fibre-reinforced composites, a higher fibre area fraction would be required.

3. In the SiC fibre-reinforced alumina matrix composites, an additional toughening mechanism occurs due to the small COD in the vicinity of the fibres which allows grain bridging to be effective at applied stress intensity factors far exceeding the critical stress intensity factor K_c of the monolithic alumina.

Acknowledgements

The author is indebted to L. Braun for assisting at the SEM and H. Xu for the sample preparation. This work was partially supported by the Department of Energy, Office of Industrial Technology under Contract No. DE A C05-840 R21400.

References

1. Y. W. MAI and B. R. LAWN, *J. Amer. Ceram. Soc.* **70** (1987) 289.
2. P. L. SWANSON, C. J. FAIRBANKS, B. R. LAWN, Y. W. MAI and B. J. HOCKEY, *ibid.* **70** (1987) 279.
3. G. VEKINIS, M. F. ASHBY and P. W. BEAUMONT, *Acta Metall.* **38** (1990) 1151.
4. S. T. BENNISON and B. R. LAWN, *ibid.* **37** (1989) 2659.
5. P. CHANTIKUL, S. J. BENNISON and B. R. LAWN, *J. Amer. Ceram. Soc.* **73** (1990) 2419.
6. D. B. MARSHALL and A. G. EVANS, *ibid.* **68** (1985) 225.
7. D. B. MARSHALL, B. N. COX and A. G. EVANS, *Acta Metall.* **33** (1985) 2013.
8. P. F. BECHER, *J. Amer. Ceram. Soc.* **73** (1991) 255.
9. P. F. BECHER, E. R. FULLER, JR. and P. ANGELINI, *ibid.* **74** (1991) 2131.
10. C. P. OSTERTAG, *J. Amer. Ceram. Soc.* in press.
11. *Idem.*, *Comp. Engng* **5** (1995) 1317.
12. J. RODEL, J. F. KELLY, M. R. STOUDT and S. J. BENNISON, *Scanning Microsc.* **5** (1991) 29.
13. B. N. COX, *Acta Metall.* **39** (1991) 1189.
14. H. TADA, P. C. PARIS and G. R. IRWIN, "The Stress Analysis Handbook" (Paris Productions (and Del Research Corp.) St. Louis, MO, 1985) Chapter 2.
15. P. CHANTIKUL, S. J. BENNISON and B. R. LAWN, *J. Amer. Ceram. Soc.* **73** (1990) 2419.
16. G. R. IRWIN, in "Handbuch der Physik", Vol. 6 edited by S. Flugge (Springer Verlag, Berlin, 1958) p. 551.
17. D. B. MARSHALL and B. N. COX, *Acta Metall.* **35** (1987) 2607.
18. H. H. XU, C. P. OSTERTAG, L. M. BRAUN and I. K. LLOYD, *J. Amer. Ceram. Soc.* **77** (1994) 1899.
19. *Idem.*, *ibid.* **77** (1994) 1897.

Received 17 July
and accepted 23 October 1996